Atomistic Structure of Cobalt–Phosphate Nanoparticles for Catalytic Water Oxidation

ARTICLE *in* ACS NANO · NOVEMBER 2012

Impact Factor: 12.88 · DOI: 10.1021/nn3044325 · Source: PubMed

4 AUTHORS, INCLUDING:

Simone Piccinin
Italian National Research Council
42 PUBLICATIONS **428** CITATIONS
SEE PROFILE

Stefano Fabris
Italian National Research Council
75 PUBLICATIONS **5,840** CITATIONS
SEE PROFILE

Atomistic Structure of Cobalt-Phosphate Nanoparticles for Catalytic Water Oxidation

Xiao Liang Hu, Simone Piccinin, Alessandro Laio,* and Stefano Fabris*

CNR-IOM Istituto Officina dei Materiali, Centro DEMOCRITOS, Scuola Internazionale Superiore di Studi Avanzati (SISSA), and Italian Institute of Technology (IIT-SISSA Unit), Via Bonomea 265, I-34136, Trieste, Italy

ABSTRACT Solar-driven water splitting is a key photochemical reaction that underpins the feasible and sustainable production of solar fuels. An amorphous cobalt-phosphate catalyst (Co-Pi) based on earth-abundant elements has been recently reported to efficiently promote water oxidation to protons and dioxygen, a main bottleneck for the overall process. The structure of this material remains largely unknown. We here exploit *ab initio* and classical atomistic simulations combined with metadynamics to build a realistic and statistically meaningful model of Co-Pi nanoparticles. We demonstrate the emergence and stability of molecular-size ordered crystallites in nanoparticles initially formed by a disordered Co−O network and phosphate groups. The stable crystallites consist of bis-oxo-bridged Co centers that assemble into layered structures (edge-sharing CoO_6 octahedra) as well as in corner- and face-sharing cubane units. These layered and cubane motifs coexist in the crystallites, which always incorporate disordered phosphate groups at the edges. Our computational nanoparticles, although limited in size to ∼1 nm, can contain more than one crystallite and incorporate up to 18 Co centers in the cubane/layered structures. The crystallites are structurally stable up to high temperatures. We simulate the extended X-ray absorption fine structure (EXAFS) of our nanoparticles. Those containing several complete and incomplete cubane motifs—which are believed to be essential for the catalytic activity—display a very good agreement with the experimental EXAFS spectra of Co-Pi grains. We propose that the crystallites in our nanoparticles are reliable structural models of the Co-Pi catalyst surface. They will be useful to reveal the origin of the catalytic efficiency of these novel water-oxidation catalysts.

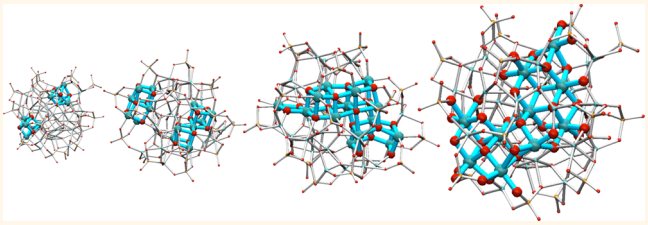

KEYWORDS: cobalt-phosphate catalyst · nanoparticle structure · water splitting · metadynamics · force field for metal oxides

Solar-driven water splitting is a key photochemical reaction in solar fuel production.[1] Precious metal oxides, such as RuO_2 and IrO_2, efficiently catalyze water oxidation—the main bottleneck for the overall process—but a realistic impact on large-scale energy conversion requires novel catalysts based on earth-abundant elements. A class of such materials—cobalt-phosphate (Co-Pi), cobalt-borate, nickel-borate, and others[2−13]—has been recently discovered and successfully applied to artificial leaf technologies. Their activity relies on ordered and oxidation-resistant active centers embedded in amorphous grains.[2−13] A well-defined structural model of these active centers would be essential for rationalizing experimental findings and for studying the reaction mechanism, but it is at present lacking due to the complex structure and composition of the grains.

Co-Pi self-assembles on conductive substrates *via* electrolysis from a phosphate-buffered Co^{2+} solution. Besides being formed by earth-abundant elements, this material is a very promising water-oxidation catalyst for technological applications because its formation and operation require a very low overpotential, room temperature, and neutral pH.[2,3] The phosphate electrolyte is supposed to play a role in facilitating proton transfer and catalyst self-repair.[3−5] Electron paramagnetic resonance (EPR) and electrokinetic studies have shown that water oxidation takes place at the oxidized $Co^{3+/4+}$ centers.[7,10] Knowing the exact structure of the active catalytic sites would be fundamental information for clarifying the reaction mechanisms. Two independent extended X-ray absorption fine structure spectroscopy (EXAFS) studies agree on the presence of discrete multiple cobalt-oxo molecular units arranged into an amorphous

* Address correspondence to fabris@sissa.it; laio@sissa.it.

Received for review May 30, 2012 and accepted November 12, 2012.

Published online November 12, 2012
10.1021/nn3044325

network.[6,8] The structure of these molecular units is presently debated. X-ray diffraction shows no sign of crystalline phases but broad amorphous features.[2] While it is clear that cobalt ions are on average coordinated by six oxygen ions forming octahedral CoO_6 units, refs 6 and 8 propose different arrangements of such units, both compatible with the Fourier-transformed EXAFS spectra. These data are interpreted in terms of either clusters of complete and incomplete vertex-sharing cobalt-oxo cubane motifs[6] or layered edge-sharing CoO_6 octahedra.[8] Extended layered edge-sharing models were shown to reproduce very well X-ray scattering data and pair distribution function analysis, which also indicate that the typical domain size of the Co-Pi grains is ~13 Å.[9] The proposed cubane arrangements displays remarkable structural analogies to the Mn_3CaO_4 core of the oxygen-evolving complex in photosystem II.[14,15] Metal centers arranged in cubane motifs have been identified in several molecular and crystalline artificial water-oxidation catalysts,[16−20] and there are indications that these ordered motifs are the active core of the amorphous Co-Pi catalysts.[17]

We here exploit *ab initio* and classical atomistic simulations combined with metadynamics[21] to build a realistic and statistically meaningful model of Co-Pi grains. Our calculations predict the formation of molecular size crystallites in heterogeneous nanoparticles initially comprising a disordered Co−O network and PO_4 units. The crystallites are composed of a combination of planar edge-sharing CoO_6 octahedra and Co_4O_4 cubane motifs, which are believed to be essential for catalytic activity.[6,16−20,22,23] The crystallites are stable, always expose cobalt sites at the surface, and incorporate phosphate groups at their edges. The simulated EXAFS spectra of our nanoparticles are compared with the *in situ* EXAFS measurements for Co-Pi grains. The good agreement demonstrates that the crystallites in our nanoparticles incorporate the main structural motifs of the Co-Pi catalyst.

RESULTS AND DISCUSSION

We simulate a set of nanoparticles containing phosphate and potassium ions in the $Co_{40}P_{20}K_{20}O_{120}$ stoichiometry, which is consistent with the ~2:1:1 ratio for Co:P:K resulting from microanalytical elemental analysis of the Co-Pi catalyst.[2] The number of oxygen atoms was determined so as to impose the charge neutrality of the particles, assuming that the formal valences are +3, +5, +1, and −2 for Co, P, K, and O ions, respectively. As it would be hopeless generating realistic structures for this large system directly by *ab initio* molecular dynamics starting from random ion positions, we first fitted an empirical potential with a shell model functional form[24,25] using *ab initio* geometries and energies of a few selected structures. Our fitted empirical potential is capable of correctly reproducing the relative energies and structural parameters of well-known cobalt oxides, resulting from the density functional theory (DFT-PBE) calculations (see Methods and Supporting Information). Most importantly, this empirical potential is reliable also for Co-Pi amorphous nanoparticles, since it predicts radial distribution functions (RDFs) for all pairs in good agreement with DFT-PBE structures (see Figure 1e−g).

Structural Model of Co-Pi Grains. Starting from random ionic positions in the computational nanoparticles, the structure and the local environment around the Co ions were first optimized with empirical potential metadynamics simulations employing two collective variables (CVs), which allowed sampling the short-range atomic environment around the Co sites: (CV1) the coordination number of Co with respect to O ions and (CV2) the number of Co ions bridging between a pair of O ions (see Methods). This computational approach allowed us to calculate the free energy of Co-Pi grains in the configurational domain spanned by CV1 and CV2 (Figure.1a). The free energy landscape displays a clear low-energy basin, which identifies a large number of putative amorphous grain structures. A subset of these lowest energy structures resulting from this initial prescreening (red points and arrows in Figure 1a) was then optimized at 0 K with empirical potential and with spin-polarized DFT-PBE calculations (see Methods). The calculated RDFs for three representative Co-Pi grains (Figure 1e−g) show that the differences between structures optimized at the classical and at the DFT level are systematically small, further indicating the high predictive power of our fitted empirical potential. The local environment of cobalt ions in these optimized structures (Figure 1b−d) is consistent with EXAFS data, namely, a predominant 6- and 5-fold coordination by oxygen ions in interlinked octahedral cobalt-oxo units. One surprising result of the simulations is the presence of nanocrystallites consisting of complete and incomplete Co_4O_4 cubane motifs in some grain candidates (*e.g.*, grain 3 in Figure 1d), despite the lack of any CV driving their formation. This suggests a thermodynamic driving force to form such local ordered arrangements of CoO_6 octahedra in the amorphous network.

In order to validate and provide further evidence of this finding, we performed a second set of empirical potential metadynamics simulations, which aimed at generating nanoparticles containing a larger fraction of cubane units. The CV used here was specifically developed for this work and is defined by the product of six pairs of coordination numbers to control the number of cubane motifs (see CV3 in Methods and Supporting Information). This computational approach allowed us to generate a large number of Co-Pi nanoparticles containing, besides the octahedral CoO_6 units, several crystallites of up to nine complete cubane motifs. A selection of these structures was then optimized at 0 K

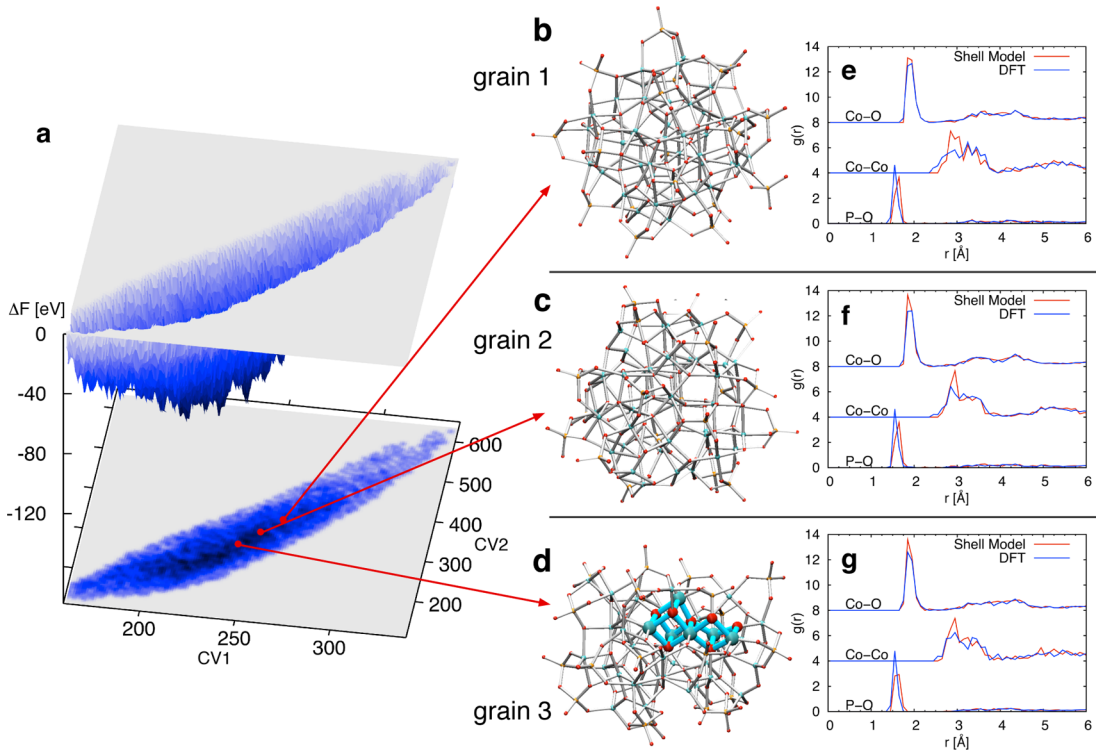

Figure 1. Models of Co-Pi grains identified with shell model metadynamics. (a) Free energy landscape of Co-Pi grains in the configurational domain spanned by the CV1 and CV2 collective variables. (b–d) Three grain structures representative of the low-energy basin. (e–g) Radial distribution functions corresponding to grains 1–3, calculated from the optimized positions predicted by shell-model (red) and DFT (blue) simulations. Co, P, and selected O ions are represented by cyan, orange, and red spheres. Larger spheres in grain 3 highlight the layered and cubane motif.

first with the empirical potential and then by spin-polarized DFT-PBE calculations (see Methods). Three representative examples of the optimized grains obtained using this procedure are displayed in Figure 2a–e. Also in this case, the differences in RDFs between the optimized structures obtained with empirical and *ab initio* methods are small. During this structural optimization, the rearrangement in the local environment around the bis-oxo-bridged Co atoms reduced the size and number of the crystallites, leading to an overall decrease of the number of complete cubane motifs from 7–9 (as in the nanoparticles obtained directly from the last metadynamics run) to 3–4 in several nanoparticle candidates. A common feature of the cubane motifs withstanding structural optimization is their proximity to the phosphates, which share at least one of their oxygen ions with the cubane structures. Quite importantly, these relaxed structures are still in the low free-energy basin previously identified. All grains are approximately spherical, and more than half of the cobalt ions are surrounded by five or six oxygen ions forming octahedral units, as evinced from EXAFS spectroscopy.[6,8] All the residual crystallites are composed of complete and incomplete cubane motifs arising from edge-sharing CoO_6 octahedra and displaying bis-oxo-bridged Co ions. The crystallites' edges are decorated by PO_4 groups and connected to a disordered Co–O network of distorted/incomplete octahedra and tetrahedra. These units fill the interstitial regions among the crystallites in the bulk of the nanoparticles and reach the nanoparticle surface. In all the nanoparticles, phosphate and potassium ions are segregated on the surface.

Morphology and Thermal Stability of the Crystallites. The nanoparticles displayed in Figure 2a–e contain crystallites with two (grain 4), three (grain 5), and four (grain 6) complete cubane motifs. In particular, grain 5 contains two corner-sharing and one isolated cubane motifs, while all the complete cubane units in grain 6 are connected and face-sharing.

In addition, these grains contain also edge-sharing cobaltate planar structures based on the incomplete cubane motif (Figure 2b,d and Figures S2 and S3 in the Supporting Information) similar to those proposed from EXAFS and high-energy X-ray scattering.[8,9] In most cases, the complete and incomplete cubane arrangements coexist in the same nanoparticle or even in the same crystallite. As an example, grain 5 contains the molecular cobaltate cluster proposed in ref 8 to be a model for surface Co-Pi (see also Figure S3 in the Supporting Information). Two surface defects are present above and below this planar cobalt dioxide layer and form the two corner-sharing, complete Co_4O_4 cubane units in grain 5 (Figure S3d in the Supporting Information). Similarly, the two cubane units in grain 4 (Figure 2a) arise from adding out-of-plane Co ions to

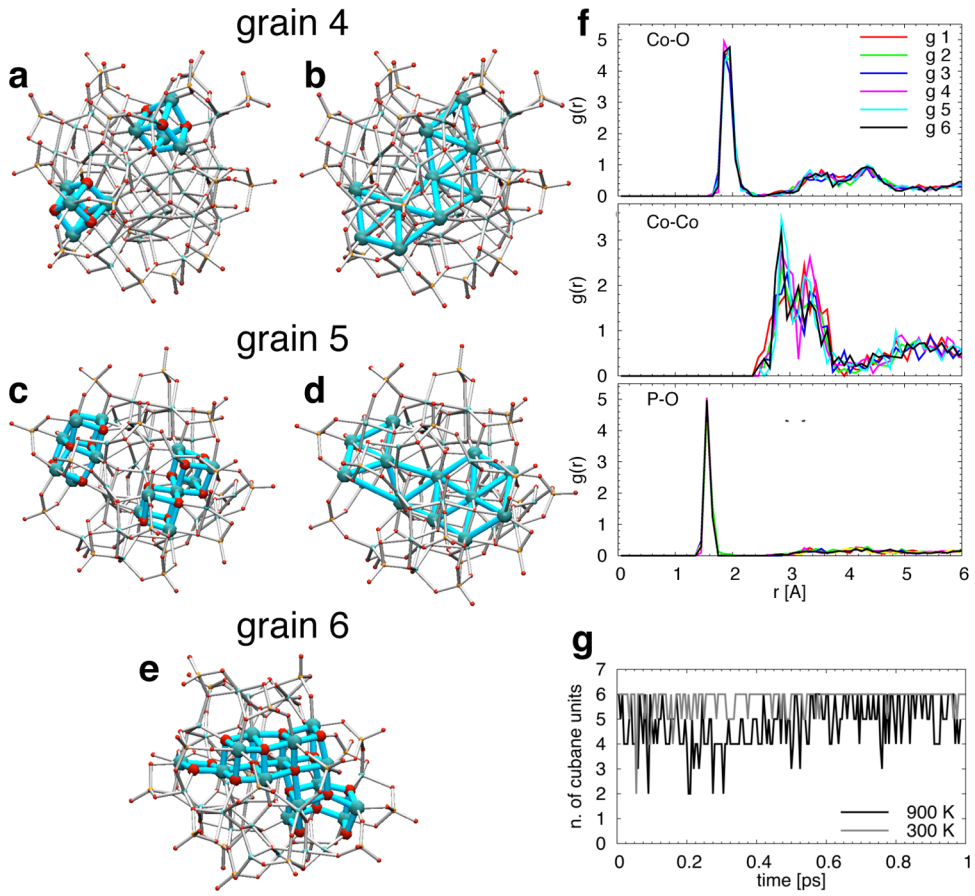

Figure 2. Structural analysis of cubane-rich Co-Pi model grains. Representative DFT-optimized grains containing two (a), three (c), and four (e) complete cubane motifs. Co ions arranged in layered cobaltite structures in grains 4 (b) and 5 (d). See also Supporting Information, Figures S2 and S3. The grains were identified with metadynamic simulations employing CV1, CV2, and CV3 (see text). (f) Radial distribution function for all grains 1−6 (abbreviated as g 1−6 in the legend). (g) Time-evolution of the number of cubane motifs in grain 6 during shell model molecular dynamics simulations.

the cobaltite-based crystallite (Figure 2b and Figure S2c in the Supporting Information). This suggest that realistic models of Co-Pi are likely to contain *both* planar cobaltite structures and interconnected cubane motifs rather than just one of these structural units. This is compatible with X-ray pair distribution function analysis, which proposes Co-Pi models incorporating cubane-type Co_4O_4 units at the edge of cobaltite sheet layers.[9]

Empirical potential molecular dynamics calculations demonstrate that the cubane motifs constituting our crystallites are stable at temperatures up to at least 900 K, as shown for the specific case of grain 6 in Figure 2e. In 1 ns of molecular dynamic simulation, the number of cubane units oscillates between 6 and 5 at 300 K and between 6 and 4 at 900 K. We therefore conclude that these crystallites present in our Co-Pi nanoparticles are structurally stable at room temperature and survive even at significantly higher temperatures.

Local Structure around Co Ions. Although the six grain structures differ in number and arrangement of complete/incomplete cubane motifs (Figures 1 and 2), they share some common features in the geometrical and electronic structures. First we notice that the RDFs for the grains with and without cubane motifs are remarkably similar (Figure 2f). In particular, the Co−Co RDF displays a broad distribution in the 2−4 Å range, while the Co−O and P−O RDFs reveal sharp peaks at 2.0 and 1.6 Å, respectively. The coordination numbers of Co and P computed from these data are ∼5.4 and ∼4. This is in agreement with the EXAFS data, which indicate a Co−O bond length of 1.89 Å and a coordination number of 5.2−6.2.[6,8] The variation of the Co−O and P−O RDFs among the six grains is very small, while that of the Co−Co RDF is larger, thus showing that the structural differences among the grains are mostly due to how rigid Co-oxo units are connected. Indeed, although there is no clear Co−Co first shell, the grains containing a larger number of cubane motifs (grains 5 and 6 in Figure 2) display an enhanced peak at ∼2.8 Å (Figure 2f). The same peak in the RDF calculated for the crystallites in grains 5 and 6 is considerably sharper and clearly centered at ∼2.8 Å (Figure S5, Supporting Information). This is precisely the Co−Co and O−O distance in a square planar arrangement of Co and O with a ∼2.0 Å Co−O side, resulting in two oxygen ions bridging a pair of cobalt ions. These bis-oxo-bridged Co

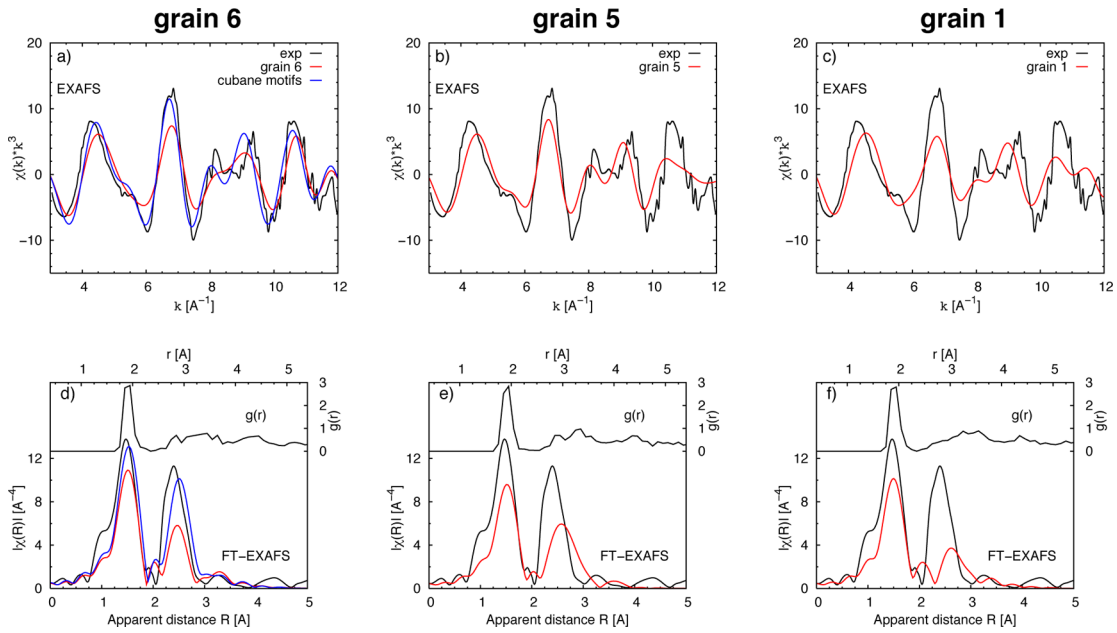

Figure 3. EXAFS spectra and Fourier transforms for three grain candidates compared to experimental ones in ref 8. Upper panel: Averaged Co k^3-weighted EXAFS oscillation over all Co ions in the grain (red line) and over only the Co ions in the cubane crystallites (blue line). Lower panel: Fourier transforms of the averaged k-space oscillation along with the radial distribution function of all Co ions with all ions in the grain. For Fourier transforms of the k^3-weighted EXAFS oscillation, the k-range of 3−12 Å and a Hanning window function were used.

ions are the building blocks of the cubane motifs as well as of the layered structures that have been proposed in refs 6, 8, and 9. Quite importantly, such putative structures were not identified directly with crystallographic measurements, but were proposed on the basis of structural parameters (average coordination numbers and interatomic distances between Co−O and Co−Co pairs) resulting from fitting the EXAFS spectra of Co-Pi catalysts.

In the following we use a direct procedure to assess the atomistic structure of the catalyst. Namely, we start from the atomic coordinates of our Co-Pi nanoparticles, and we simulate the corresponding EXAFS spectra by calculating the phases and amplitudes in the EXAFS equation (see Methods) and compare them with the experimental data. Besides assessing the accuracy of our model for Co-Pi clusters, the comparison allows for rationalizing the spectroscopic measurements, providing insights into the origins of the different spectral features.

Comparison with EXAFS Spectra and Discussion. The top panels of Figure 3 display the simulated Co k^3-weighted EXAFS spectra calculated for different nanoparticles containing four (grain 6, panel a), three (grain 5, panel b), and zero (grain 1, panel c) complete cubane motifs. The red lines refer to simulated spectra obtained by averaging the EXAFS signal over all the Co ions in the nanoparticle. The simulated spectra are compared to the experimental spectrum (black line in all panels) measured for a Co-Pi thick film and reported in ref 8. The corresponding Fourier transforms of these spectra are reported in the bottom panels (d−f) of Figure 3. The theoretical spectra for the nanoparticles richest in crystallites and cubane motifs, grains 5 and 6, display an overall good agreement with the experimental spectrum, in both the position and width of the main peaks. Instead, significant differences with experiment affect the simulated EXAFS spectrum of amorphous nanoparticles without cubane motifs (grain 1). We first focus our analysis on grain 6, having the largest cubane crystallites. The RDF of Co ions with all surrounding ions for grains 6 is also reported in Figure 3d. The first-shell experimental peak (at ∼1.5 Å, black line) is present both in the Fourier-transformed EXAFS spectra (at ∼1.5 Å, red line) and in the RDF (at ∼2.0 Å). It clearly corresponds to the Co−O bond length at ∼2.0 Å, which is also consistent with high-energy X-ray scattering data (1.91 Å).[9] The second experimental peak (at ∼2.4 Å, black line) is qualitatively well reproduced by the simulated spectra (at ∼2.5 Å, red line), but its relative height with respect to the first peak is underestimated by ∼30% with reference to experiment. As already noticed, the RDF also shows a broad second peak between ∼2.5 and ∼4 Å, which reflects the broad distribution of Co−Co distances in the disordered fraction of the grain. Remarkably, the shoulder is almost completely absent in the Fourier transform of the EXAFS spectrum computed for the same grain, which in turn is, as we already underlined, consistent with experiment, except for the relative height of the second peak. This suggests that the peak of the transformed EXAFS at the apparent distance of ∼2.4 Å arises mostly from the quasi-ordered portion of the grain, namely, from Co pairs bridged by two

oxygens, as in cubane units or layered structures. As already noticed, this peak has a correspondence in the RDF at a Co−Co distance of ∼2.89 Å, in good agreement with the X-ray pair distribution function analysis (2.82 Å).[9] The contribution from Co pairs linked by one oxygen only is clearly filtered out in the transformed EXAFS spectrum, possibly due to the broader distribution of their distance in an amorphous sample. Indeed a second peak in the simulated FT EXAFS spectrum is also present for grain 5 (Figure 3e), which contains a lower number of cubane motifs, but is almost absent for grain 1 (Figure 3f), which contains no ordered Co−O clusters.

This comparison clearly shows that the larger the number of cubane motifs in our nanoparticles, the better the agreement with the experimental EXAFS data and suggests that our computational nanoparticles contain a marginally smaller fraction of ordered cubane/layered motifs than Co-Pi. With the chosen simulation setup it was not possible to stabilize larger crystallites in the model nanoparticles, and this is likely due to size effects, open boundary conditions, local-minima trapping during the minimization, or inaccuracies in the force field. Although the fraction of amorphous region in our small nanoparticles might be overestimated with respect to the actual material, regions of our nanoparticles abundant in cubane motifs and terminated by their neighboring phosphate groups well reproduce all the known experimental features of the Co-Pi catalyst. This is demonstrated by the very good agreement with experiment of the EXAFS spectra calculated for the fraction of grain 6 containing the cubane motifs and the neighboring O ions and phosphate groups (blue line in Figure 3). In addition, the presence of disordered PO_4 groups at the edge of our crystallites (see Supporting Information Figure S5, a and b) is compatible with local models proposed by X-ray pair distribution function analysis (*e.g.*, model 4 in ref 9). Computational mechanistic studies of this reaction have so far considered oversimplified minimal structural models of Co-Pi.[22,23] We propose that the stable crystallite *surface* in our grains is likely to be a reliable representative of the surface of the real catalyst. It can therefore be used as a more realistic model structure for investigating the catalytic properties of Co-Pi.

Spin State of Co Ions in Different Environments. All the grains display approximately the same ratio among the number of CoO_4, CoO_5, and CoO_6 units. In particular, ∼30−50% of the Co ions are octahedrally 6-fold coordinated and constitute primarily the bulk of the crystallites. The remaining Co ions belong to distorted/incomplete octahedra (∼30−50%) and tetrahedra (<∼20%) units that terminate the crystalline edges and/or constitute the amorphous region between crystallites (Figure 4). The electronic structure of the grains resulting from our DFT-PBE calculations displays a metallic character (see Supporting Information, Figure S6). The use of hybrid exchange−correlation functionals or of DFT+U methods can improve this description but will have minor effects on the structural properties of our grains. The calculations identify a clear correlation between the local environments around Co ions and the spin polarization. The calculated spin density displayed in Figure 4 shows that tetrahedral CoO_4 or distorted CoO_5 environments determine the emergence of a net spin polarization (purple isosurface), while the Co^{3+} ions in the perfect octahedral CoO_6 units of the cubane-rich crystallites are low spin. This is consistent with EPR measurements indicating that the Co^{3+} centers in an octahedral field prefer to be low-spin.[7] The emergence of paramagnetic signals in Co-Pi films may have two contributions: one due to the distorted local environments in the disordered region of the grain comprising tetrahedral CoO_4 or distorted CoO_5 units (crystallite boundaries and surfaces), the other due to the oxidation of the Co ions in octahedral coordination to Co^{4+} species. The latter effect is at the basis of the interpretation of EPR signals in Co-Pi films, namely, the formation of Co^{4+} species during water oxidation under the application of an external bias.[7]

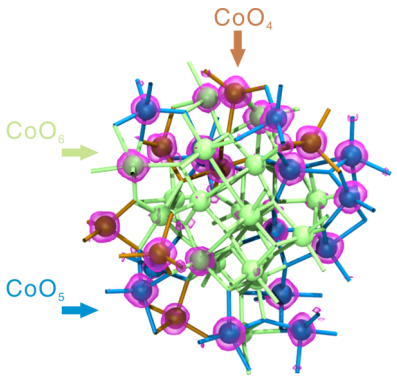

Figure 4. Correlation between net spin polarization and local Co atomic environment. Net spin density ($|\rho_{up} - \rho_{down}|$) calculated for grain 6 and plotted with isosurfaces of $|\pm 0.05|$ electron/bohr^3. Brown, blue, and green colors identify the CoO_4, CoO_5, and CoO_6 units, respectively.

Our calculations show that, at zero bias, the Co ions in the cubane motifs are in an almost perfect octahedral environment and should therefore be EPR-silent Co^{3+} species. Under an external bias, some of them will cycle to higher oxidation states, leading to the emergence of the EPR-active Co^{4+} species. Paramagnetic $[Co(III)_3Co(IV)O_4]$ cubane intermediates have indeed been proposed as compatible with the paramagnetic signals measured on Co-Pi films during water oxidation.[17]

CONCLUSIONS

The functionality of the Co-Pi water-oxidation catalysts relies on both the structure and chemical composition around the Co active sites. Mechanistic studies based on electrokinetic experiments suggest a one-electron one-proton reaction mechanism that involves Co^{3+}−OH and Co^{4+}−O moieties,[10] which are likely

located within cubane units. The reaction is proposed to be assisted by neighboring phosphate groups, either in solution or surface bound, that act as proton acceptors. Due to the difficulties in determining realistic structures of ordered metal-oxo sites embedded in heterogeneous amorphous grains, reliable structural and compositional models of the active sites involved in these processes are missing. The mechanistic studies available so far assumed minimal functional models consisting of one or a few interconnected cubane motifs.[22,23] These computational works neglected the presence of phosphate groups, their effect on the local structure, and their role into the reaction mechanism. The structures of the crystallites predicted by our simulations open new opportunities for understanding the functionality of these catalysts. Besides providing direct evidence of the formation of stable crystallites comprising complete/incomplete cubane molecular units, our calculations show that these layered cobaltite structures coexist with corner- and face-sharing cubane motifs in the same crystallite. Moreover we provide atomistic models for the crystallite edges, which expose Co ions and incorporate disordered PO_4 groups at the nanoparticle surface.

These findings have several important implications. The presence of surface phosphate groups near the active Co sites will likely affect the reaction mechanism. Incomplete surface cubane units are plausible adsorption sites for dynamical phosphate exchange with the electrolyte. The proximity between cubane motifs and phosphates also suggests that the latter might act as proton acceptors as surface-bound species. Phosphates will also affect directly the protonation of the neighboring oxygen ions, the formation of oxo and hydroxo groups, and the occurrence of protonated μ-oxo bridges.[23] In summary, we believe the structural models of the Co-Pi nanoparticles proposed in this work will allow for a more quantitative approach to reveal the water-oxidation mechanism promoted by these materials.

COMPUTATIONAL METHODS

Fitting of Empirical Potential. The empirical potential adopted in this work is the shell model potential,[24,25] as implemented in GULP[26] and DL_PLOY 2.[27] The oxygen ion has a shell (O_s) of charge Y and a core (O_c) of charge (z-Y), coupled by a harmonic spring (k):

$$V_{cs} = 1/2kr_{cs}^2$$

Each cation has a formal charge of z only. The interaction between ions at a distance r_{ij} is modeled by

$$V_{ij} = A\exp(-r_{ij}/B) + z_i z_j/r_{ij}$$

Since no parameters for Co-Pi are available in the literature, we generated them by fitting DFT-PBE energy and geometry for well-known oxides (Co_3O_4 and K_3PO_4). We proceed as follows. We first run a few different molecular dynamics trajectories at 300 K with some trial parameters. Then, for a few randomly chosen configurations, we compute energy and forces at the DFT-PBE level, and we fit the parameters to match these values. This procedure can be iterated. The parameters obtained in this manner are listed in Table S1 (see Supporting Information). As shown in Figure S1 (see Supporting Information), our empirical potential is able to reproduce the relative energies among structures with remarkable accuracy, even for structures that are not used for the fitting. The lattice constants of the fitted shell model are presented in Table S2 (see Supporting Information), and the shell model lattice constants are within 3.5% of the DFT-PBE values. The shell model is also capable of reproducing the DFT-PBE RDFs of the Co−O, Co−Co, and P−O pairs in amorphous Co-Pi grains (see Figure 1).

Metadynamics Calculations. We perform metadynamics[21] using DL_PLOY 2[27] and PLUMED[28] to investigate the formation and stability of CoO_6 octahedra and cubane motifs in Co-Pi. The first two CVs for metadynamics are defined as

$$\mathrm{CV1} = \sum_{i\in \mathrm{Co}} \sum_{j\in \mathrm{O}} f_{R_0,n,m}(r_{ij})$$

where

$$f_{R_0,n,m}(r_{ij}) = \frac{1-(r_{ij}/R_0)^n}{1-(r_{ij}/R_0)^m}$$

with $n = 4$, $m = 8$, and $R_0 = 2.25$ Å, and

$$\mathrm{CV2} = \sum_{i\in \mathrm{Co}} \sum_{\substack{j,k\in \mathrm{O} \\ k>j}} [f_{R_0,n,m}(r_{ij})\, f_{R_0,n,m}(r_{ik})]$$

with $n = 8$, $m = 16$, and $R_0 = 2.25$ Å. Performing metadynamics with these two CVs can lead arbitrarily generated initial structures to relatively compact spherical structures, containing several octahedral CoO_x units. The third CV is designed to control the cubane motifs, defined as the product of six neighboring cobalt pairs in the cubic cobalt-oxo unit:

$$\mathrm{CV3} = \sum_{\substack{i,j,k,l\in \mathrm{Co} \\ i<j<k<l}} [f_{R_0,n,m}(r_{ij})\cdot f_{R_0,n,m}(r_{ik})\cdot f_{R_0,n,m}(r_{il})\cdot f_{R_0,n,m}(r_{jk})\cdot f_{R_0,n,m}(r_{jl})\cdot f_{R_0,n,m}(r_{kl})]$$

with $n = 60$, $m = 120$, and $R_0 = 3.15$ Å. In Figure S4 (see Supporting Information), we show the number of cubane motifs as a function of time in three independent metadynamics trajectories performed with this setup.

DFT Calculations. A few structures with different number of cubane motifs are chosen from our metadynamics simulations and optimized at the spin-polarized DFT level, with the PBE exchange−correlation functional,[29] ultrasoft pseudopotentials, and Γ point sampling of the Brillouin zone. A cutoff of 30 Ry is used for the plane wave basis set. In the geometry optimization, the grains are simulated in a periodical cubic supercell of 25 Å, and the forces on each ion are converged to ≤0.025 eV/Å. The DFT calculations are performed with the Quantum ESPRESSO code.[30]

EXAFS Calculations. The k-space EXAFS spectra $\chi_i(k)$ for each Co ion in the grains are calculated with the FEFF 9 code[31,32] separately. The atomic coordinates from optimized spin-polarized DFT-PBE calculations are used in the FEFF input files. The damping factor (S_0^2) is set to 0.75, consistent with the value used in ref 8. The Debye−Waller factor is set to zero. We checked that using other values proposed in the literature leads to variations in the spectra that are small with respect to the discrepancy between experimental and computational spectra. The potential with the Hedin−Lundqvist exchange−correlation functional involved in $\chi_i(k)$ is calculated self-consistently. The averaged k-space oscillation is obtained by

$$\chi(k) = \sum_i \chi_i(k)/N$$

where N is the number of Co ions in the specific group (*i.e.*, all the Co ions in the grain or only the Co ions belonging to the cubane motifs). Fourier transform of the k-space oscillation is performed with the ATHENA code in the IFEFFIT package. A Hanning window function is used to cover the k-range of 3−12 Å.

Conflict of Interest: The authors declare no competing financial interest.

Acknowledgment. We thank G. Scoles for prompting our interest in this topic and for reading the manuscript, and G. Aquilanti for assistance in the interpretation of the XAS data and for useful discussions. We acknowledge the CINECA Award No. HP10B8FMFJ, 2010, for the availability of high-performance computing resources and support. S.F. acknowledges the COST action CM1104 "Reducible Oxide Chemistry, Structure, and Functions" for support.

Supporting Information Available: Fitting and testing of the shell model parameters for Co-Pi; atomistic structures of crystallites in grains 4, 5, and 6; metadynamics trajectories using CV3; calculated radial distribution functions restricted to crystallites; total and projected density of electronic states for grain 6; and coordinates of the grains in Figures 1 and 2. This material is available free of charge *via* the Internet at http://pubs.acs.org.

REFERENCES AND NOTES

1. Lewis, N. S.; Nocera, D. G. Powering the Planet: Chemical Challenges in Solar Energy Utilization. *Proc. Natl. Acad. Sci.* **2006**, *103*, 15729–15735.
2. Kanan, M. W.; Nocera, D. G. In Situ Formation of an Oxygen-Evolving Catalyst in Neutral Water Containing Phosphate and Co^{2+}. *Science* **2008**, *321*, 1072–1075.
3. Kanan, M. W.; Surendranath, Y.; Nocera, D. G. Cobalt-Phosphate Oxygen-Evolving Compound. *Chem. Soc. Rev.* **2009**, *38*, 109–114.
4. Surendranath, Y.; Dincă, M.; Nocera, D. G. Electrolyte-Dependent Electrosynthesis and Activity of Cobalt-Based Water Oxidation Catalysts. *J. Am. Chem. Soc.* **2009**, *131*, 2615–2620.
5. Lutterman, D. A.; Surendranath, Y.; Nocera, D. G. A Self-Healing Oxygen-Evolving Catalyst. *J. Am. Chem. Soc.* **2009**, *131*, 3838–3839.
6. Risch, M.; Khare, V.; Zaharieva, I.; Gerencser, L.; Chernev, P.; Dau, H. Cobalt-Oxo Core of a Water-Oxidizing Catalyst Film. *J. Am. Chem. Soc.* **2009**, *131*, 6936–6937.
7. McAlpin, J. G.; Surendranath, Y.; Dincă, M.; Stich, T. A.; Stoia, S. A.; Casey, W. H.; Nocera, D. G.; Britt, R. D. EPR Evidence for Co(IV) Species Produced during Water Oxidation at Neutral pH. *J. Am. Chem. Soc.* **2010**, *132*, 6882–6883.
8. Kanan, M. W.; Yano, J.; Surendranath, Y.; Dincă, M.; Yachandra, V. K.; Nocera, D. G. Structure and Valency of a Cobalt-Phosphate Water Oxidation Catalyst Determined by in Situ X-ray Spectroscopy. *J. Am. Chem. Soc.* **2010**, *132*, 13692–13701.
9. Du, P.; Kokhan, O.; Chapman, K. W.; Chupas, P. J.; Tiede, D. M. Elucidating the Domain Structure of the Cobalt Oxide Water Splitting Catalyst by X-ray Pair Distribution Function Analysis. *J. Am. Chem. Soc.* **2012**, *134*, 11096–11099.
10. Surendranath, Y.; Kanan, M. W.; Nocera, D. G. Mechanistic Studies of the Oxygen Evolution Reaction by a Cobalt-Phosphate Catalyst at Neutral pH. *J. Am. Chem. Soc.* **2010**, *132*, 16501–16509.
11. Dincă, M.; Surendranath, Y.; Nocera, D. G. Nickel-Borate Oxygen-Evolving Catalyst That Functions under Benign Conditions. *Proc. Natl. Acad. Sci.* **2010**, *107*, 10337–10341.
12. Surendranath, Y.; Lutterman, D. A.; Liu, Y.; Nocera, D. G. Nucleation, Growth, and Repair of a Cobalt-Based Oxygen Evolving Catalyst. *J. Am. Chem. Soc.* **2012**, *134*, 6326–6336.
13. Bediako, D. K.; Lassalle-Kaiser, B.; Surendranath, Y.; Yano, J.; Yachandra, V. K.; Nocera, D. G. Structure-Activity Correlations in a Nickel-Borate Oxygen Evolution Catalyst. *J. Am. Chem. Soc.* **2012**, *134*, 6801–6809.
14. Ferreira, K. N.; Iverson, T. M.; Maghlaoui, K.; Barber, J.; Iwata, S. Architecture of the Photosynthetic Oxygen-Evolving Center. *Science* **2004**, *303*, 1831–1838.
15. Umena, Y.; Kawakami, K.; Shen, J.-R.; Kamiya, N. Crystal Structure of Oxygen-Evolving Photosystem II at a Resolution of 1.9 Å. *Nature* **2011**, *473*, 55–60.
16. Symes, M. D.; Surendranath, Y.; Lutterman, D. A.; Nocera, D. G. Bidirectional and Unidirectional PCET in a Molecular Model of a Cobalt-Based Oxygen-Evolving Catalyst. *J. Am. Chem. Soc.* **2011**, *133*, 5174–5177.
17. McAlpin, J. G.; Stich, T. A.; Ohlin, C. A.; Surendranath, Y.; Nocera, D. G.; Casey, W. H.; Britt, R. D. Electronic Structure Description of a $[Co(III)_3Co(IV)O_4]$ Cluster: A Model for the Paramagnetic Intermediate in Cobalt-Catalyzed Water Oxidation. *J. Am. Chem. Soc.* **2011**, *133*, 15444–15452.
18. McCool, N. S.; Robinson, D. M.; Sheats, J. E.; Dismukes, G. C. A Co_4O_4 "Cubane" Water Oxidation Catalyst Inspired by Photosynthesis. *J. Am. Chem. Soc.* **2011**, *133*, 11446–11449.
19. Gardner, G. P.; Go, Y. B.; Robinson, D. M.; Smith, P. F.; Hadermann, J.; Abakumov, A.; Greenblatt, M.; Dismukes, G. C. Structural Requirement in Lithium Cobalt Oxides for the Catalytic Oxidation of Water. *Angew. Chem., Int. Ed.* **2012**, *51*, 1616–1619.
20. Jiao, F.; Frei, H. Nanostructured Cobalt Oxide Clusters in Mesoporous Silica as Efficient Oxygen-Evolving Catalysts. *Angew. Chem., Int. Ed.* **2009**, *48*, 1841–1844.
21. Laio, A.; Parrinello, M. Escaping Free-Energy Minima. *Proc. Natl. Acad. Sci.* **2002**, *99*, 12562–12566.
22. Wang, L.-P.; Van Voorhis, T. Direct-Coupling O_2 Bond Forming a Pathway in Cobalt Oxide Water Oxidation Catalysts. *J. Phys. Chem. Lett.* **2011**, *2*, 2200–2204.
23. Mattioli, G.; Risch, M.; Bonapasta, A. A.; Dau, H.; Guidoni, L. Protonation States in a Cobalt-Oxide Catalyst for Water Oxidation: Fine Comparison of *Ab Initio* Molecular Dynamics and X-ray Absorption Spectroscopy Results. *Phys. Chem. Chem. Phys.* **2011**, *13*, 15437–15441.
24. Dick, B. G.; Overhauser, A. W. Theory of the Dielectric Constants of Alkali Halide Crystal. *Phys. Rev.* **1958**, *112*, 90–103.
25. Lewis, G. V.; Catlow, C. R. A. Potential Models for Ionic Oxides. *J. Phys. C: Solid State Phys.* **1985**, *18*, 1149–1161.
26. Gale, J. D.; Rohl, A. L. The General Utility Lattice Program. *Mol. Simul.* **2003**, *29*, 291–341.
27. Smith, W.; Forester, T. R. DL_POLY_2.0: A General-Purpose Parallel Molecular Dynamics Simulation Package. *J. Mol. Graph.* **1996**, *14*, 136−141.
28. Bonomi, M.; Branduardi, D.; Bussi, G.; Camilloni, C.; Provasi, D.; Raiteri, P.; Donadio, D.; Marinelli, F.; Pietrucci, F.; Broglia, R. A.; *et al.* PLUMED: A Portable Plugin for Free-Energy Calculations with Molecular Dynamics. *Comput. Phys. Commun.* **2009**, *180*, 1961–1972.
29. Perdew, J. P.; Burke, K.; Ernzerhof, M. Generalized Gradient Approximation Made Simple. *Phys. Rev. Lett.* **1996**, *77*, 3865–3868.
30. Giannozzi, P.; Baroni, S.; Bonini, N.; Calandra, M.; Car, R.; Cavazzoni, C.; Ceresoli, D.; Chiarotti, G. L.; Cococcioni, M.; Dabo, I.; *et al.* QUANTUM ESPRESSO: A Modular and Open-Source Software Project for Quantum Simulations of Materials. *J. Phys.: Condens. Matter* **2009**, *21*, 395502.
31. Rehr, J. J; Kas, J. J; Prange, M. P.; Sorini, A. P.; Takimoto, Y. *Ab Initio* Theory And Calculations of X-ray Spectra. *C. R. Phys.* **2009**, *10*, 548–559.
32. Rehr, J. J.; Albers, R. C. Modern Theory of XAFS. *Rev. Mod. Phys.* **2000**, *72*, 621–654.